RESEARCH PAPER

Design, Molecular Docking and *In Silico* Evaluation of Benzimidazole Derivatives as Potential Quorum Sensing Inhibitors

Apoorva A. Bankar[1], Vaishali P. Nagulwar[2], Nazma N. Inamdar[1]*

[1]*Government College of Pharmacy, Amravati, Maharashtra 444604, India*
[2]*Government College of Pharmacy, Chhatrapati Sambhajinagar, Maharashtra 431005, India*
***Corresponding author:** Dr. Nazma N. Inamdar, nazmainamdar@gmail.com*

ABSTRACT
The phenomenon of quorum sensing (QS) plays a critical role in the regulation of virulence and pathogenicity of *Pseudomonas aeruginosa*. Among the various QS systems of *P. aeruginosa*, the LasR-mediated signaling pathway plays a major role in regulating virulence factor production and biofilm development. In the present study, a series of benzimidazole derivatives (**BIM1-57**) was designed and evaluated *in silico* as potential quorum sensing inhibitors targeting the LasR receptor protein. Molecular docking studies showed that benzimidazole derivatives demonstrated strong binding affinities and interactions with key active-site residues of LasR. Comparative interaction analysis suggested that structural modifications on the benzimidazole scaffold significantly influenced binding interactions. Moreover, molecular property and drug-likeness evaluation indicated acceptable pharmacokinetic profiles for the selected compounds. Based on docking scores, interaction patterns, and predicted molecular properties, the most promising derivatives were identified for further synthesis and biological evaluation as potential antivirulence agents targeting bacterial quorum sensing.

Keywords: Benzimidazole; Quorum sensing; LasR; Molecular docking; *Pseudomonas aeruginosa*; *in silico* studies
How to cite this article: Bankar AA, Nagulwar VP, Inamdar NN. Design, Molecular Docking and In Silico Evaluation of Benzimidazole Derivatives as Potential Quorum Sensing Inhibitors. Int J Drug Deliv Technol. 2026;16(60): 1049-1060. DOI: 10.25258/ijddt.16.60.116
Source of support: Nil.
Conflict of interest: None.

1. INTRODUCTION

The growing prevalence of drug-resistant bacterial infections has created an urgent need for alternative therapeutic approaches beyond conventional antibiotics. Among resistant pathogens, *P. aeruginosa* infection remains particularly challenging due to the organism's intrinsic resistance mechanisms, remarkable adaptability, and ability to form persistent biofilms[1]. This pathogen is associated with a wide range of acute and chronic infections, particularly in immunocompromised patients, and is frequently implicated in hospital-acquired infections. In addition to antibiotic resistance, the pathogenicity of *P. aeruginosa* is closely linked to the production of multiple virulence factors and its ability to establish persistent biofilms, both of which further complicate treatment and contribute to therapeutic failure[2].

Quorum sensing (QS) is a bacterial cell-to-cell communication mechanism that regulates collective behaviours in response to population density through the production and detection of small signaling molecules known as autoinducers[3]. In *P. aeruginosa*, the Las quorum sensing system serves as a major regulatory network controlling several virulence-associated phenotypes, including biofilm formation, pyocyanin production, motility, and secretion of extracellular enzymes. The transcriptional regulator LasR is activated upon binding with its natural signaling molecule N-(3-oxododecanoyl)-L-homoserine lactone (OdDHL, **Figure 1**), leading to the expression of QS-regulated genes[4]. Since quorum sensing regulates bacterial virulence rather than bacterial survival directly, inhibition of this system has emerged as an attractive antivirulence strategy that may reduce the selective pressure associated with traditional antibiotics and potentially minimize the development of resistance[5].

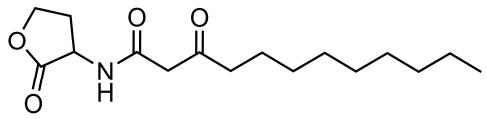

OdDHL

Figure 1. Structure of OdDHL, the native autoinducer of LasR transcriptional regulator.

Among the various approaches explored for QS inhibition, the design of small molecules capable of disrupting LasR-mediated signaling has attracted considerable attention[6]. Consequently, several synthetic scaffolds have been investigated as potential LasR antagonists. Among these, benzimidazole has emerged as a promising pharmacophore, with numerous benzimidazole-based derivatives reported to exhibit significant QS inhibitory activity (**Figure 2**).

1.1. Reported benzimidazole derivatives as quorum sensing inhibitors

Benzimidazole-based scaffolds have attracted considerable attention as quorum sensing inhibitors owing to their ability to modulate multiple QS regulatory pathways in *P. aeruginosa* and related

*Author for Correspondence: nazmainamdar@gmail.com

bacterial systems (**I-VII**, **Figure 2**). Among the early examples, a benzamide–benzimidazole derivative M64 (**I**) was reported by Rahme and co-workers as a potent MvfR inhibitor that suppressed pyocyanin production in *P. aeruginosa* PA14 with an IC_{50} of 0.6 μM[7,8]. Subsequently, 5,6-dimethyl-2-aminobenzimidazole (**II**) was identified as a LasR inhibitor active against *P. aeruginosa* PAO-JP2 and PAO-JG21 with IC_{50} values of 2.3 and 1.4 μM, respectively[9]. Further scaffold expansion by Srinivasarao *et al.*[10] led to triazole-linked 2-aminobenzimidazoles (**III**) that inhibited LasR-dependent GFP expression in *P. aeruginosa*, while another benzimidazole analogue (**IV**) exhibited inhibition of violacein production in *Chromobacterium violaceum* CV026 with an IC_{50} of 36.67 μM[11]. A moderately potent benzimidazole derivative (**V**) was reported by Abd El-Aleam *et al.*[12], that inhibited QS-regulated virulence factors in *P. aeruginosa* at 24.19 μM. More recently, Soukarieh *et al.*[13] developed a highly potent benzo[d]imidazole-based PqsR antagonist (**VI**) active against both *P. aeruginosa* PAO1 and PA14 with submicromolar IC_{50} values (0.07–0.09 μM). Along similar lines, Mohammed *et al.*[14] identified another highly potent benzo[d]imidazole derivative (**VII**) as a LasR inhibitor capable of suppressing biofilm formation, pyocyanin production, and motility with an IC_{50} of 0.74 μM. Collectively, these studies highlight the benzimidazole scaffold as a versatile and promising chemotype for the development of quorum sensing-targeted antivirulence agents.

Encouraged by these findings, benzimidazole was selected as the core scaffold in the present study for the design of new potential quorum sensing inhibitors targeting the LasR receptor protein. A series of benzimidazole derivatives was therefore designed and evaluated *in silico* for their potential to inhibit LasR-mediated quorum sensing. Molecular docking studies were performed to investigate the binding affinity and interaction profiles of the designed compounds within the LasR ligand-binding domain. In addition, molecular property and drug-likeness analyses were carried out to evaluate their pharmacokinetic suitability and drug-like potential.

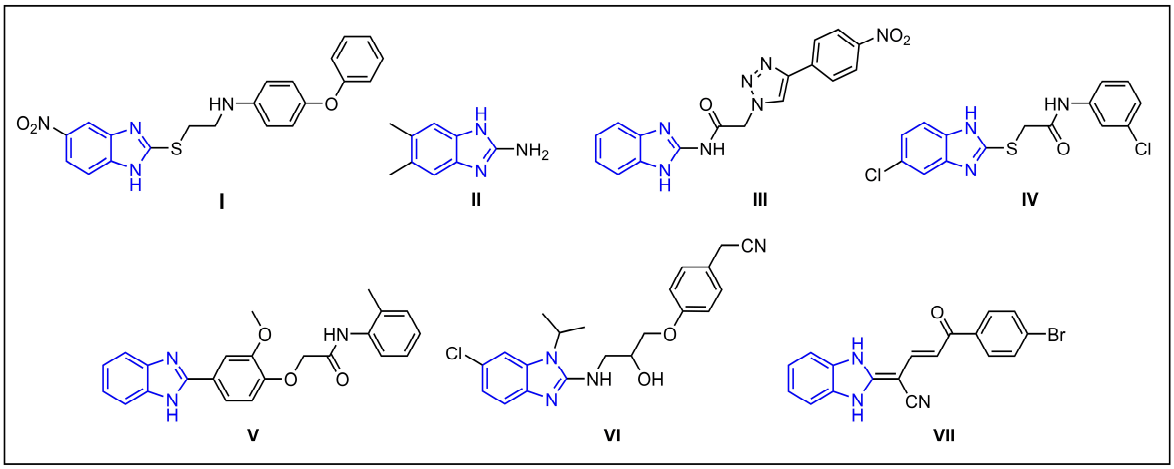

Figure 2. Benzimidazole-based quorum sensing inhibitors (**I-VII**).

2. MATERIALS AND METHODS

2.1. Retrieval of Protein Structures

The crystallographic structure of the selected target protein LasR was retrieved from the RCSB Protein Data Bank (https://www.rcsb.org). A total of five crystal structures of LasR co-crystallized with its native ligand OdDHL were identified in PDB and are summarized in **Table 1**. Among these, the structure with PDB ID 3IX3 was selected for the present study owing to its high crystallographic resolution (1.4 Å) and well-defined ligand-binding pocket, making it highly suitable for molecular docking and interaction analysis studies.

Table 1. Crystal structures of LasR available in PDB.

Year	PDB ID	Co-crystallized Ligand	Resolution (Å)
2007	2UVO	OdDHL	1.8
2009	3IX3	OdDHL	1.4
2021	6V7W	OdDHL	3.0
2013	4NG2	OdDHL	2.41
2020	6V7X	OdDHL	2.90

2.2. Protein Preparation

The crystal structure of the LasR complexed with its native autoinducer OdDHL was retrieved from the

Protein Data Bank (PDB ID: **3IX3**). Prior to molecular docking studies, the protein structure was prepared using the Protein Preparation Wizard in Schrodinger Suites. Since the crystal structure exists as a homodimer, only Chain A was retained for docking studies, while Chain B was deleted. The protein structure was subsequently processed using the Preprocess module to assign bond orders, add hydrogen atoms, create disulfide bonds, and resolve crystallographic inconsistencies. Protonation and ionization states of amino acid residues at physiological pH (7.0 ± 2.0) were generated using the Epik module. Hydrogen-bond assignments and optimization of protonation states were performed using PROPKA at pH 7.0, including sampling of water orientations to obtain an energetically favourable hydrogen-bonding network. Crystallographic water molecules distant from the active site were removed; however, one water molecule involved in water-mediated hydrogen-bonding interaction with the native ligand was retained. Finally, restrained energy minimization was performed using the Impref module with the OPLS-2003 force field until the heavy atom RMSD converged to 0.3 Å.

2.3. Ligand Preparation

The structures of the designed compounds were drawn using ChemDraw and saved in SDF format. Ligand preparation was carried out using the LigPrep module. The imported ligands were processed to generate three-dimensional structures, and geometry optimization was performed using the OPLS-2003 force field. Possible ionization and protonation states at physiological pH (7.0 ± 2.0) were generated using the Epik module. Appropriate chiralities were retained during ligand preparation, and low-energy conformations of the ligands were generated for subsequent molecular docking studies.

2.4. Grid generation

The Receptor Grid Generation module of Glide was employed to generate the grid for molecular docking. The co-crystallized ligand OdDHL present in the LasR crystal structure was used as the reference for defining the binding site. A receptor grid box of 20 × 20 × 20 Å was generated around the centroid of OdDHL.

2.5. Molecular Docking

The docking protocol was validated by redocking of co-crystallized ligand into the active site, yielding an RMSD of 0.457 Å relative to the crystallographic pose. The energy optimized ligands were docked using Ligand Docking module of Glide using the Standard Precision (SP) docking mode with the OPLS-2003 force field. Ligands were ranked by Glide docking score and protein–ligand interactions were analyzed.

2.6. Molecular Properties

The molecular properties of the designed benzimidazole derivatives were evaluated *in silico* to assess their physicochemical characteristics, drug-likeness, and pharmacokinetic suitability. Various molecular descriptors, including molecular weight, lipophilicity, hydrogen bond donors and acceptors, topological polar surface area, and aqueous solubility, were calculated using the QikProp module of Schrodinger. In addition, the compounds were analyzed for their compliance with Lipinski's rule of five. Predicted ADME-related properties such as gastrointestinal absorption and blood–brain barrier permeability were also assessed.

3. DESIGN

Understanding the mode of binding of the natural ligand within the ligand-binding domain provides important insight into the structural features required for effective receptor antagonism. Thus, to design compounds as potential LasR antagonists, the structural characteristics of the LasR receptor and its interactions with the native autoinducer OdDHL were first analyzed.

3.1. Analysis of LasR Ligand Binding Domain

The structural basis of ligand recognition in LasR was understood from the crystal structure of the ligand-binding domain of *P. aeruginosa* in which LasR was co-crystallized with its native autoinducer OdDHL. Activated LasR exists as a symmetrical homodimer, where each monomer accommodates one ligand molecule within a deeply enclosed binding cavity (**Figure 3**)[15]. Binding of OdDHL stabilizes the LasR ligand-binding domain and promotes formation of the active dimeric conformation, thereby enabling subsequent binding of the DNA-binding domain to specific promoter regions regulating quorum sensing-controlled genes.

Detailed examination of the ligand-binding site revealed OdDHL makes five hydrogen-bonding interactions within the binding pocket (**Figure 3**). Key residues involved in these interactions include Tyr56, Trp60, Arg61, Asp73, and Ser129. In addition, the long acyl chain of OdDHL extends into an elongated hydrophobic pocket lined predominantly by residues such as Leu36, Tyr47, Ile52, Val76, Trp88, Phe101, and Leu110. Together, these polar and hydrophobic interactions play an important role in ligand stabilization within the active site of LasR.

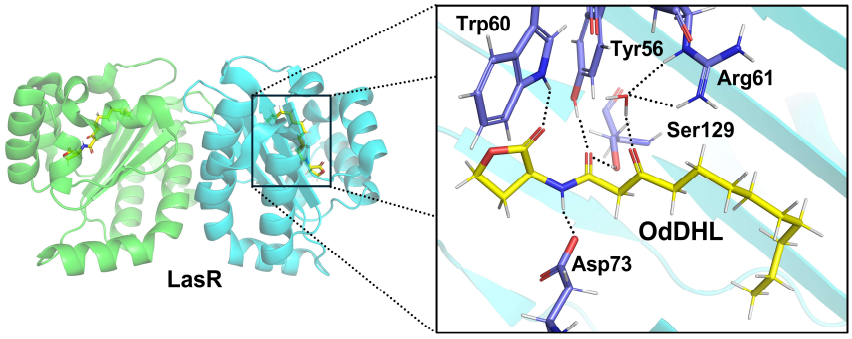

Figure 3. The LasR homodimer in complex with OdDHL. The expanded view highlights key interactions of OdDHL within the ligand-binding domain.

These structural insights provide an important framework for the rational design of small-molecule LasR antagonists capable of mimicking key interactions within the ligand-binding domain.

3.2. Rational Design of Benzimidazole derivatives as potential QSIs

The ligand-binding pocket of the LasR receptor is characterized by three distinct regions, namely an aromatic region, a polar region, and a hydrophobic region, which together contribute to ligand accommodation and stabilization within the active site[16]. With this consideration, a series of benzimidazole derivatives (**BIM1-57**) were rationally designed by incorporating three complementary pharmacophoric components (**Figure 4**). In the designed molecules, the *N,N*-dimethylbenzimidazole nucleus was intended to occupy the hydrophobic region and the heteroatoms present within the scaffold were expected to contribute to additional stabilizing interactions with nearby residues. The hydrazide linker was designed to provide conformational flexibility and facilitate hydrogen-bonding interactions within the polar region of the binding pocket. Furthermore, the terminal aromatic ring (substituted/unsubstituted) was intended to occupy the aromatic region of the binding cavity. Variations in aromatic ring and/or substitutions were introduced to explore the influence of steric, hydrophobic, and electronic variations on receptor interaction and binding affinity. Thus, the overall molecular architecture was designed to achieve complementary occupancy of the major regions of the LasR binding pocket and thereby potentially acting as quorum sensing inhibitory agents.

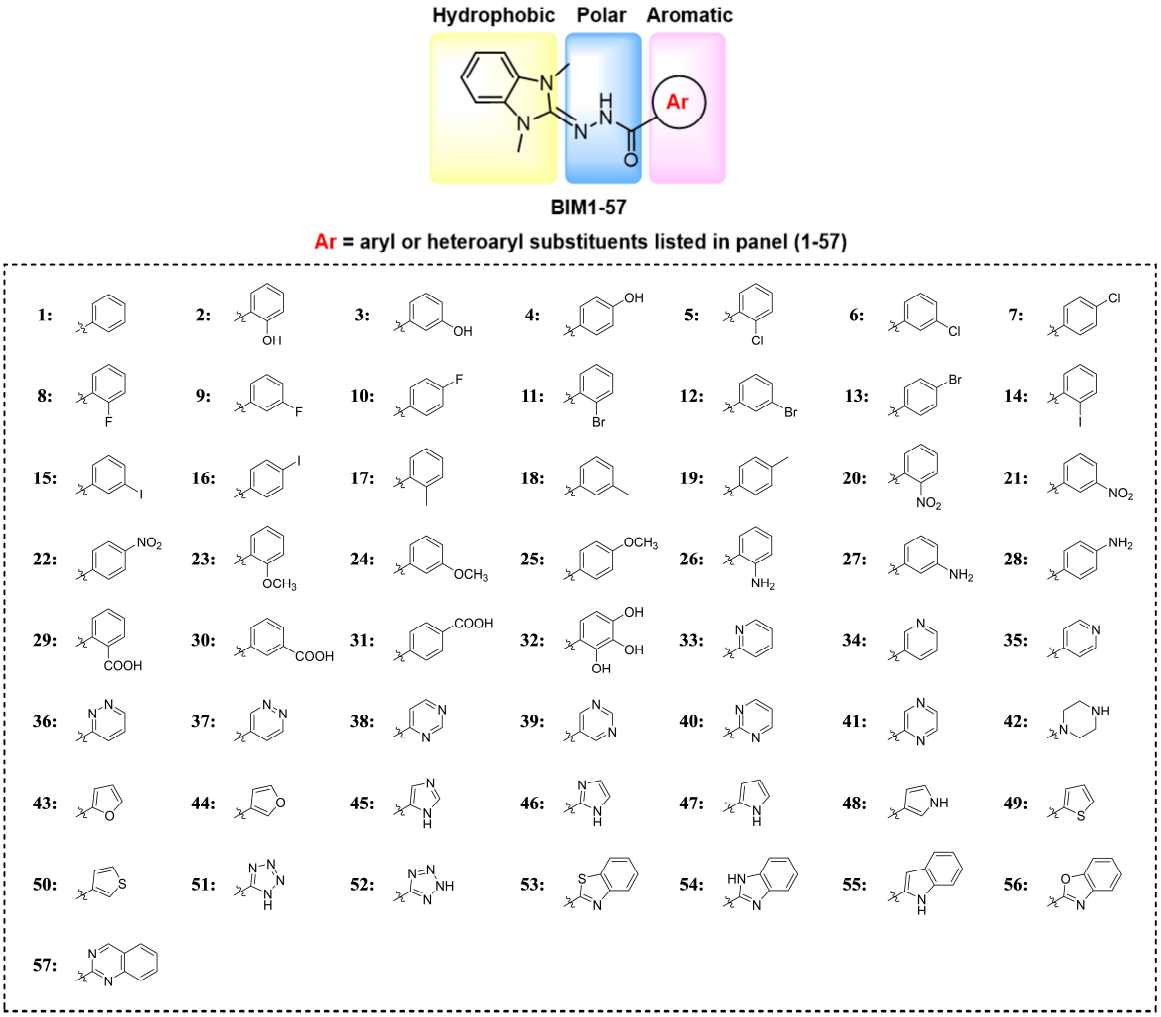

Figure 4. Rational design of benzimidazole derivatives (**BIM1-57**) as LasR-targeted quorum sensing inhibitors.

4. RESULTS AND DISCUSSION

4.1. Molecular Docking

4.1.1. Interaction analysis

Prior to docking of the designed BIM series, the docking procedure was validated by re-docking the co-crystallized autoinducer OdDHL into the ligand-binding domain of LasR. In the crystal structure, OdDHL is stabilized through a network of key interactions involving Tyr56, Trp60, Asp73, Ser129, and Arg61. The generated docked pose reproduced the experimentally observed orientation of OdDHL within the binding pocket with high accuracy, yielding an RMSD value of 0.457 Å relative to the crystallographic conformation (**Figure 5**). Furthermore, the re-docked ligand retained the characteristic interaction profile of the native complex and produced a docking score of –7.816 kcal/mol, thereby validating the reliability of the adopted docking protocol for subsequent studies.

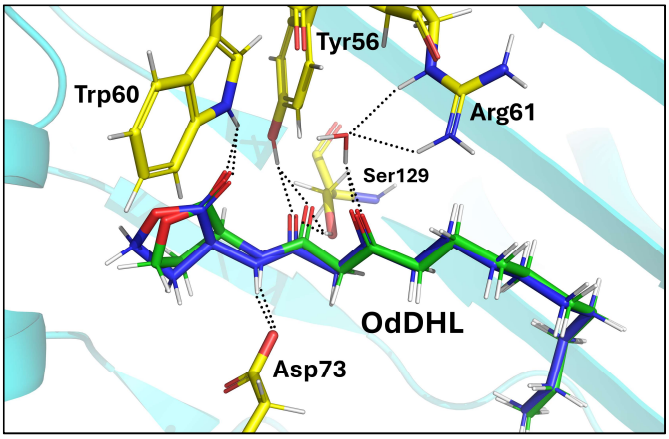

Figure 5. 3D superimposed view of the crystallographic pose of OdDHL (green) and its re-docked conformation (blue) within the LasR ligand-binding domain (RMSD = 0.457 Å).

Following validation of the docking protocol, all designed benzimidazole derivatives were docked into the ligand-binding domain of LasR to investigate their binding affinity and interaction profiles.

Analysis of the docking poses revealed that all BIM derivatives occupied the ligand-binding pocket of LasR. The docking scores ranged from −6.548 to −9.699 kcal/mol, with all compounds except **BIM32** exhibiting comparable or higher binding affinity than the native ligand OdDHL (−7.816 kcal/mol) (**Table 2**). Among the series, **BIM8** and **BIM29** demonstrated the highest docking scores of −9.699 and −9.695 kcal/mol, respectively, followed by **BIM9** (−9.430 kcal/mol), **BIM52** (−9.396 kcal/mol), **BIM54** and **BIM28** (−9.371 kcal/mol) (**Figure 6A**). These findings suggest a strong binding affinity of BIM derivatives toward the LasR ligand-binding pocket.

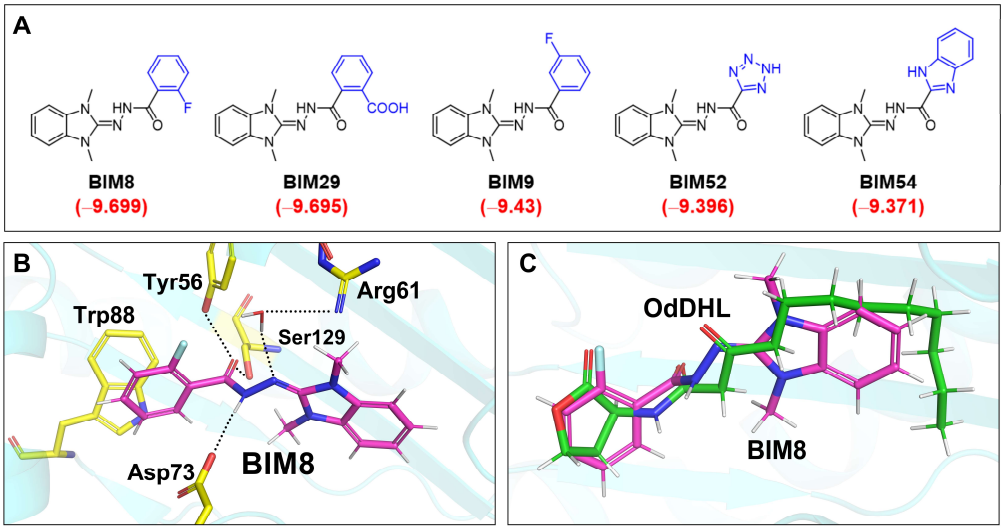

Figure 6. (A) Top five BIM derivatives arranged in descending order of docking score against the LasR active site, **(B)** Docking pose and key interactions of **BIM8** within the LasR-ligand-binding domain, **(C)** Overlay of the docked pose of **BIM8** (pink) with **OdDHL** (green) in the LasR-ligand-binding domain.

Detailed interaction analysis revealed that the compounds established interactions with several key amino acid residues within the LasR binding pocket (**Table 2**). The docking pose and key interactions of highest-scoring compound, **BIM8,** within the LasR-ligand binding domain are shown in **Figure 6B**. Overall, the BIM derivatives interacted with residues including Arg61, Asp73, Tyr56, Ser129, Trp60, Thr75, Tyr93, Leu110, Trp88, Phe101, and Tyr47. The most frequently observed hydrogen-bonding interactions involved Arg61, Asp73, Tyr56, Ser129, and Trp60, indicating their crucial role in stabilization of the LasR–BIM complexes. Additional hydrogen-bonding interactions with residues such as Thr75, Tyr93, and Leu110 were observed in selected derivatives. The π–π stacking interactions were predominantly observed with Trp88, which appeared as the major aromatic interaction residue across multiple high-scoring compounds. Other

aromatic stacking interactions involving Phe101, Tyr47, Tyr56, Asp73, and Tyr93 were observed in a limited number of derivatives. **Figure 7** illustrates the interaction maps of the top five scoring compounds (**BIM8, BIM29, BIM9, BIM52, BIM54**) within the LasR binding pocket.

Interestingly, several compounds that showed comparatively lower docking scores primarily interacted through Arg61 and Trp60, without establishing the broader interaction network observed for the top-ranked derivatives. Overall, the interaction analysis indicated that simultaneous engagement with conserved hydrogen-bonding residues along with additional aromatic interactions contributed to improved binding affinity within the LasR ligand-binding domain.

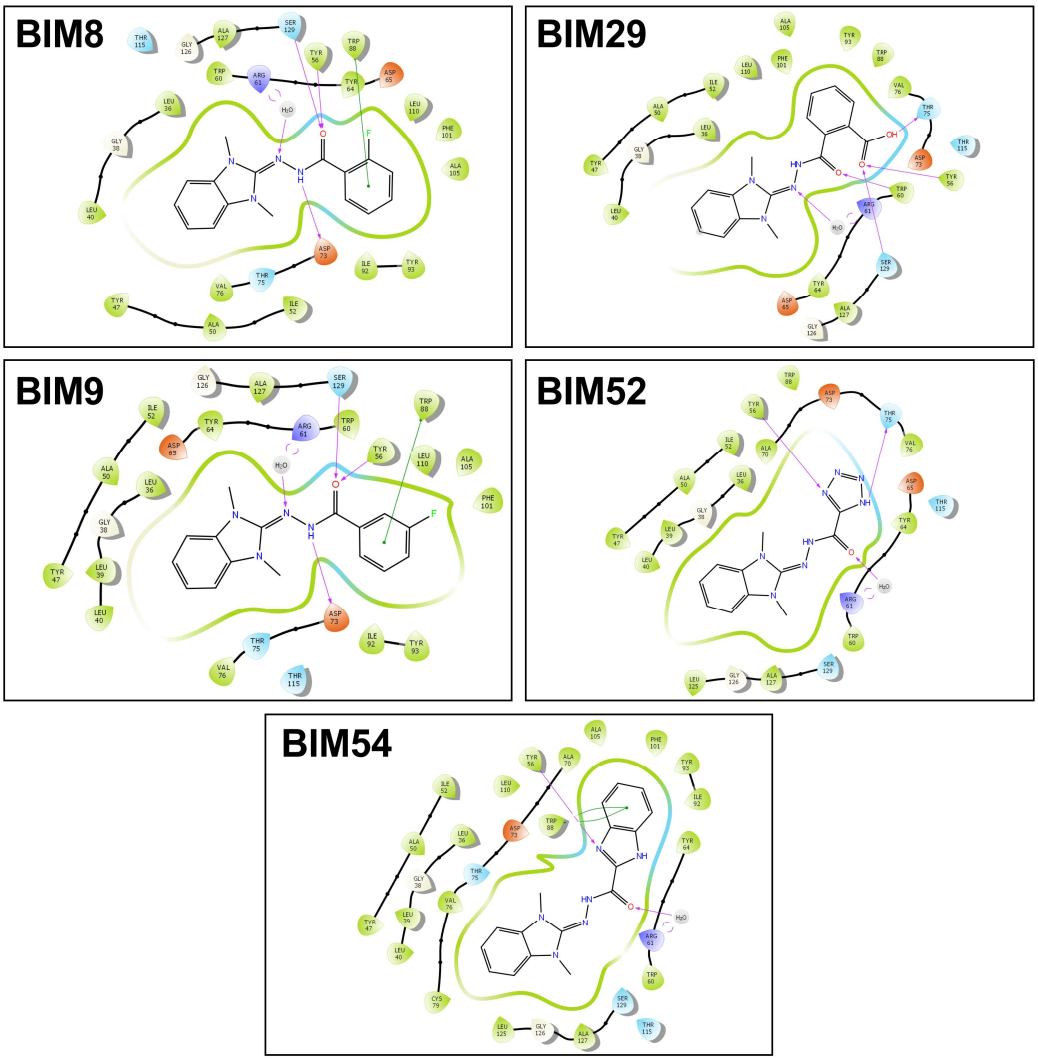

Figure 7. 2D interaction maps of the top five scoring **BIM** derivatives within the LasR binding pocket showing hydrogen bonding and π–π stacking interactions with key active-site residues.

Most importantly, the docking poses of the BIM derivatives supported the proposed design strategy, where the benzimidazole nucleus was oriented toward the hydrophobic region generally occupied by the OdDHL acyl chain, while the terminal aromatic ring was positioned within the lactone-binding region. The hydrazide linker served as a polar spacer connecting these two regions and facilitating interactions within the binding pocket. Structural superimposition of OdDHL with the top-scoring compound **BIM8** within the LasR ligand-binding domain further illustrated this comparable binding orientation (**Figure 6C**). These observations suggest that the designed benzimidazole scaffold possesses suitable structural features for effective interaction with the LasR receptor and may serve as a promising framework for the development of quorum sensing inhibitors.

Table 2. Molecular docking data of benzimidazole-hydrazides (**BIM1** to **BIM57**) against LasR. OdDHL is included as the native ligand.

ID	Ar	Docking score (kcal/mol)	Rank	Interactions	
				Hydrogen bonding	π–π stacking
OdDHL	-	−7.816	-	Tyr56, Ser129, Asp73, Trp60, Arg61	-
BIM1	C_6H_5	−9.219	8	Asp73, Arg61, Tyr56, Ser129	Trp88
BIM2	2-HOC_6H_4	−8.496	22	Arg61, Trp60, Thr75, Ser129	-
BIM3	3-HOC_6H_4	−8.856	14	Arg61, Trp60, Tyr93, Asp73	Trp88
BIM4	4-HOC_6H_4	−9.154	9	Arg61, Asp73, Leu110, Tyr56	Trp88
BIM5	2-ClC_6H_4	−8.172	31	Arg61, Trp60	-
BIM6	3-ClC_6H_4	−7.978	36	Arg61	-
BIM7	4-ClC_6H_4	−8.587	19	Asp73, Arg61, Tyr56, Ser129	-
BIM8	2-FC_6H_4	−9.699	1	Asp73, Arg61, Tyr56, Ser129	Trp88
BIM9	3-FC_6H_4	−9.43	3	Asp73, Arg61, Tyr56, Ser129	Trp88
BIM10	4-FC_6H_4	−9.225	7	Asp73, Arg61, Tyr56, Ser129	-
BIM11	2-BrC_6H_4	−8.234	27	Asp73, Arg61, Tyr56, Ser129	-
BIM12	3-BrC_6H_4	−8.059	33	Arg61	-
BIM13	4-BrC_6H_4	−8.447	24	Asp73, Arg61, Tyr56, Ser129	-
BIM14	2-IC_6H_4	−7.694	47	Arg61, Trp60	-
BIM15	3-IC_6H_4	−7.688	48	Arg61	-
BIM16	4-IC_6H_4	−8.162	32	Asp73, Arg61, Tyr56, Ser129	-
BIM17	2-$CH_3C_6H_4$	−7.9	39	Arg61, Trp60	-
BIM18	3-$CH_3C_6H_4$	−8.032	35	Asp73, Tyr56, Ser129	-
BIM19	4-$CH_3C_6H_4$	−8.986	10	Asp73, Arg61, Tyr56, Ser129	-
BIM20	2-$NO_2C_6H_4$	-	-	No stable docking pose obtained	-
BIM21	3-$NO_2C_6H_4$	−8.04	34	Arg61	Asp73, Trp88
BIM22	4-$NO_2C_6H_4$	−6.907	55	Arg61	Asp73, Trp88
BIM23	2-$OCH_3C_6H_4$	−7.829	43	Arg61, Trp60	Trp88, Phe101
BIM24	3-$OCH_3C_6H_4$	−7.89	40	Arg61, Trp60	-
BIM25	4-$OCH_3C_6H_4$	−8.405	25	Asp73, Arg61, Tyr56, Ser129	-
BIM26	2-$NH_2C_6H_4$	−8.252	26	Arg61, Trp60, Thr75	-
BIM27	3-$NH_2C_6H_4$	−8.551	20	Asp73, Arg61, Tyr56, Ser129	-
BIM28	4-$NH_2C_6H_4$	−9.371	6	Asp73, Arg61, Tyr56, Ser129	Trp88
BIM29	2-$COOHC_6H_4$	−9.695	2	Arg61, Trp60, Thr75, Tyr56, Ser129	-
BIM30	3-$COOHC_6H_4$	−7.645	49	Arg61	-
BIM31	4-$COOHC_6H_4$	−7.593	51	Arg61, Tyr93	Tyr47
BIM32	2,3,4-$(OH)_3C_6H_2$	−6.548	56	Arg61, Trp60, Thr75	Tyr47, Tyr56
BIM33	2-pyridyl	−8.183	30	Arg61, Trp60	Trp88, Phe101
BIM34	3-pyridyl	−8.835	15	Asp73, Arg61, Tyr56, Ser129	-
BIM35	4-pyridyl	−8.771	17	Asp73, Arg61, Tyr56, Ser129	-
BIM36	3-pyridazinyl	−7.868	42	Arg61, Trp60	Trp88
BIM37	4-pyridazinyl	−7.878	41	Arg61, Trp60	Trp88
BIM38	4-pyrimidinyl	−7.765	44	Arg61, Trp60, Asp73	Trp88
BIM39	5-pyrimidinyl	−8.801	16	Asp73, Arg61, Tyr56, Ser129	Trp88
BIM40	2-pyrimidinyl	−7.932	38	Arg61, Trp60	-
BIM41	2-pyrazinyl	−8.524	21	Asp73, Arg61, Tyr56, Ser129	Trp88
BIM42	piperazinyl	−7.726	45	Arg61, Trp60	Trp88, Phe101
BIM43	2-furyl	−7.628	50	Arg61, Trp60	Trp88
BIM44	3-furyl	−8.903	13	Asp73, Arg61, Tyr56, Ser129	-
BIM45	5-imidazolyl	−7.491	52	Arg61, Trp60	Trp88, Phe101
BIM46	2-imidazolyl	−7.703	46	Arg61, Trp60, Tyr93	-
BIM47	2-pyrrolyl	−8.685	18	Asp73, Arg61, Tyr56, Ser129	Trp88
BIM48	3-pyrrolyl	−7.461	53	Arg61, Trp60	Trp88
BIM49	2-thiophenyl	−8.942	12	Asp73, Arg61, Tyr56, Ser129	-
BIM50	3-thiophenyl	−8.467	23	Asp73, Arg61, Tyr56, Ser129	-
BIM51	5-tetrazolyl	−7.952	37	Arg61	Tyr56

BIM52	4-tetrazolyl	−9.396	4	Tyr56, Arg61, Thr75	-
BIM53	benzothiazolyl	−7.121	54	Arg61	Tyr56
BIM54	benzimidazolyl	−9.371	5	Tyr56, Arg61	Trp88
BIM55	indol-2-yl	−8.985	11	Arg61, Ser129	-
BIM56	benzoxazol-2-yl	−8.222	28	Arg61, Ser129	-
BIM57	quinazolin-2-yl	−8.222	29	Arg61, Ser129	-

4.1.2. Structure-binding affinity relationship

Structural diversification of the terminal aryl region revealed that the LasR binding pocket exhibited good tolerance toward a wide variety of aromatic and heteroaromatic substitutions (**Table 2**). Appreciable binding affinities were observed not only with substituted phenyl derivatives, but also with six-membered heteroaryl, five-membered heteroaryl, and fused bicyclic heterocyclic systems, indicating considerable flexibility of the binding pocket toward structurally diverse aromatic moieties. These findings suggest that multiple aromatic scaffolds can effectively occupy the aromatic region in the LasR ligand-binding domain while maintaining key stabilizing interactions with crucial residues.

Among the six-membered aromatic/heteroaromatic systems, the unsubstituted phenyl derivative (**BIM1**) exhibited the most favorable binding affinity, followed by pyridine analogues (**BIM33-35,** −8.835 to −8.183 kcal/mol), pyrimidine analogues (**BIM38-40,** −8.801 to −7.932 kcal/mol), pyrazine analogue (**BIM41**, −8.524 kcal/mol) while pyridazine derivatives (**BIM36-37**) exhibited comparatively weaker binding affinity (−7.878 to −7.868 kcal/mol) (**Figure 8A**). The overall binding affinity trend was observed as: **Phenyl > pyridine > pyrimidine > pyrazine > pyridazine.** These findings suggest that six-membered nitrogen-containing heteroaryl systems were generally well tolerated within the LasR binding pocket, although increasing nitrogen incorporation appeared to slightly reduce binding affinity. Interestingly, within a given heteroaryl ring system, the point of attachment of the ring also appeared to influence the docking affinity, as reflected by the noticeable variations in docking scores among different positional isomers of pyridine (**BIM33-35**), pyrimidine (**BIM38-40**), and pyridazine derivatives (**BIM36-37**). This indicates that not only the type of heteroaryl ring, but also its spatial orientation and positioning of nitrogen atoms, play an important role in achieving key interactions within the LasR binding pocket. Among the five-membered heterocyclic systems, the binding affinity trend was observed as: **tetrazole > thiophene > furan > pyrrole > imidazole (Figure 8B)**. The 4-tetrazole-containing derivative (**BIM52**) exhibited the most favourable docking affinity (−9.396 kcal/mol) toward the LasR ligand-binding domain, whereas imidazole derivatives (**BIM45, BIM46**) displayed comparatively weaker binding performance within this class. Similar to the observations made with six-membered heteroaryl systems, the docking affinity of five-membered heterocycles also appeared to depend not only on the nature of the ring system but additionally on the orientation and positioning of heteroatoms within the aromatic scaffold.

Among the fused bicyclic heterocyclic derivatives, benzimidazole-containing analogue (**BIM54**) demonstrated the highest docking affinity (−9.371 kcal/mol), followed by indole derivative (**BIM55**, −8.985 kcal/mol), whereas benzoxazole (**BIM56**, −8.222 kcal/mol) and quinazoline analogues (**BIM57**, −8.222 kcal/mol) exhibited comparable docking scores, and benzothiazole derivative (**BIM53**) showed comparatively lower binding affinity (−7.121 kcal/mol) (**Figure 8C**). The binding affinity trend was observed as: **benzimidazole > indole > benzoxazole ≈ quinazoline > benzothiazole.** Interestingly, the comparatively higher docking affinities observed for benzimidazole and indole derivatives may be associated with the presence of a free NH group within the fused bicyclic scaffold, which could contribute to favourable hydrogen-bonding interactions and improved stabilization within the LasR binding pocket.

Thus, among the BIM derivatives bearing unsubstituted aromatic ring systems, phenyl analogue (**BIM1**), tetrazole analogue (**BIM52**), and benzimidazole analogue (**BIM54**) emerged as the best-performing compounds within the six-membered, five-membered, and fused bicyclic aromatic categories, respectively. These observations suggest that the LasR ligand-binding pocket can accommodate structurally diverse aromatic systems, but optimal binding appears to depend on a balance between aromatic surface area, hydrogen-bonding capability, and hydrophobic complementarity within the binding cavity.

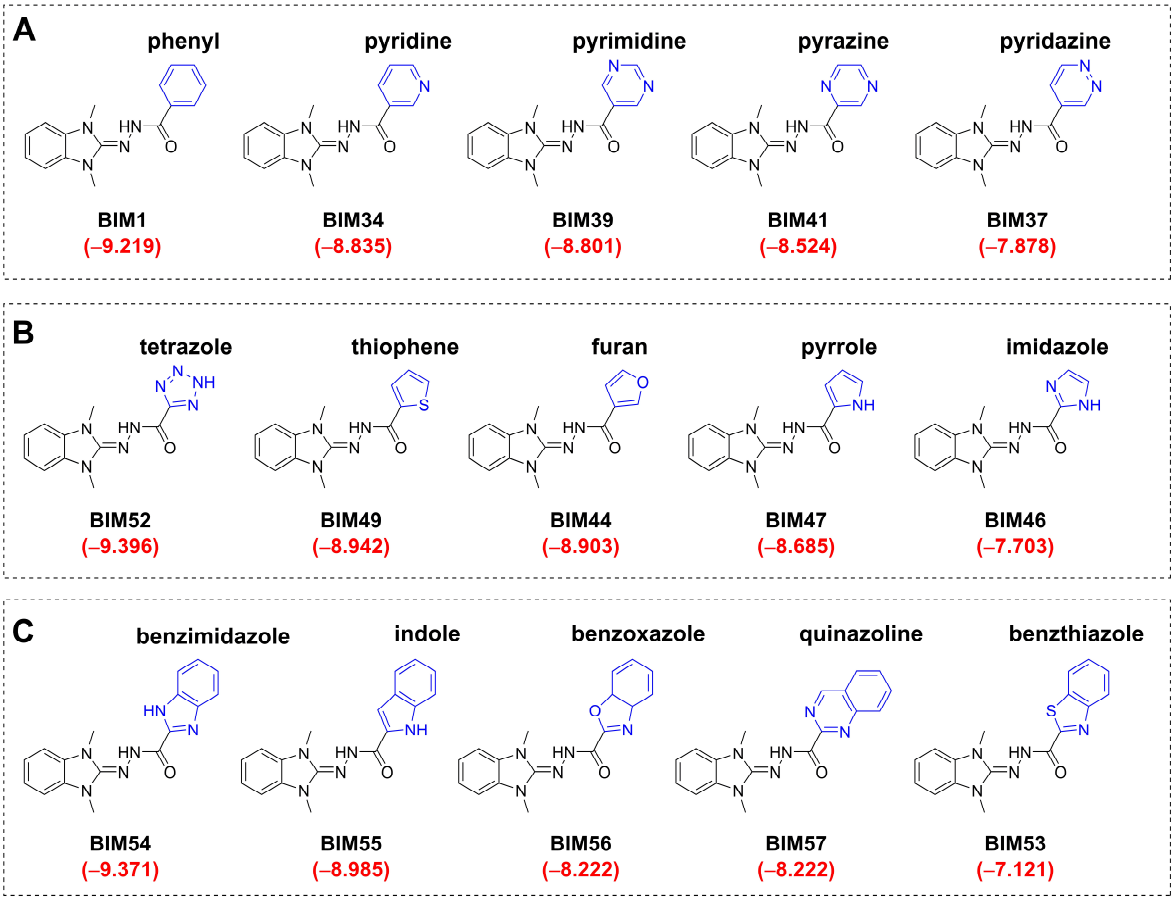

Figure 8. The observed binding affinity trends among **(A)** six-membered **(B)** five-membered, and **(C)** fused bicyclic aromatic BIM derivatives against the LasR ligand-binding domain.

Since the unsubstituted phenyl derivative **BIM1** exhibited strong docking affinity among the six-membered ring BIM analogues, the effect of phenyl ring substitution was further analyzed. Interestingly, only the ortho-fluoro derivative **BIM8** (−9.699 kcal/mol) and ortho-carboxyl derivative **BIM29** (−9.695 kcal/mol) surpassed the docking affinity of **BIM1** (−9.219 kcal/mol), whereas, the rest of the substituted phenyl analogues displayed comparatively lower docking scores (**Table 2**). The enhanced binding affinity observed for **BIM8** and **BIM29** may be associated with the ability of small or strongly polar substituents at the ortho position to promote optimal electronic interactions and additional hydrogen-bonding interactions within the aromatic region of the LasR binding pocket.

Substitution pattern analysis on the phenyl ring further revealed that both the nature of the substituent and its positional orientation significantly influenced the docking affinity toward the LasR ligand-binding domain. For electron-donating substituents, para-substituted derivatives consistently demonstrated superior docking affinity compared with the corresponding meta- and ortho-substituted analogues, following the general trend **para > meta > ortho (Table 2).** Among these electron-donating substituents at the para position, the observed docking affinity trend was: NH_2 > OH > CH_3 > OCH_3 **(Figure 9A).** This observation suggests that para substitution provides a more favourable orientation for interaction within the aromatic region of the LasR binding cavity while minimizing steric interference around the linker region. Among the electron withdrawing groups, two distinct positional trends were observed. Similar to pattern observed for electron-donating groups, chloro-, bromo- and iodo-derivatives demonstrated improved docking affinity upon para substitution, generally following the trend p > o > m **(Table 2)**. Among these para-substituted electron-withdrawing derivatives, the docking affinity trend was observed as: Cl > Br > I **(Figure 9B).** In contrast, fluoro- and carboxyl-substituted derivatives displayed a different positional preference, exhibiting the trend o > m > p. Notably, the ortho-fluoro (**BIM8**) and ortho-carboxyl (**BIM29**) analogues emerged as the two highest-scoring compounds in the entire series. This distinct behaviour may be attributed to the strong electronegative and polar nature of fluoro and carboxyl substituents, which may favour alternative binding orientations and additional stabilizing interactions when positioned at the ortho site.

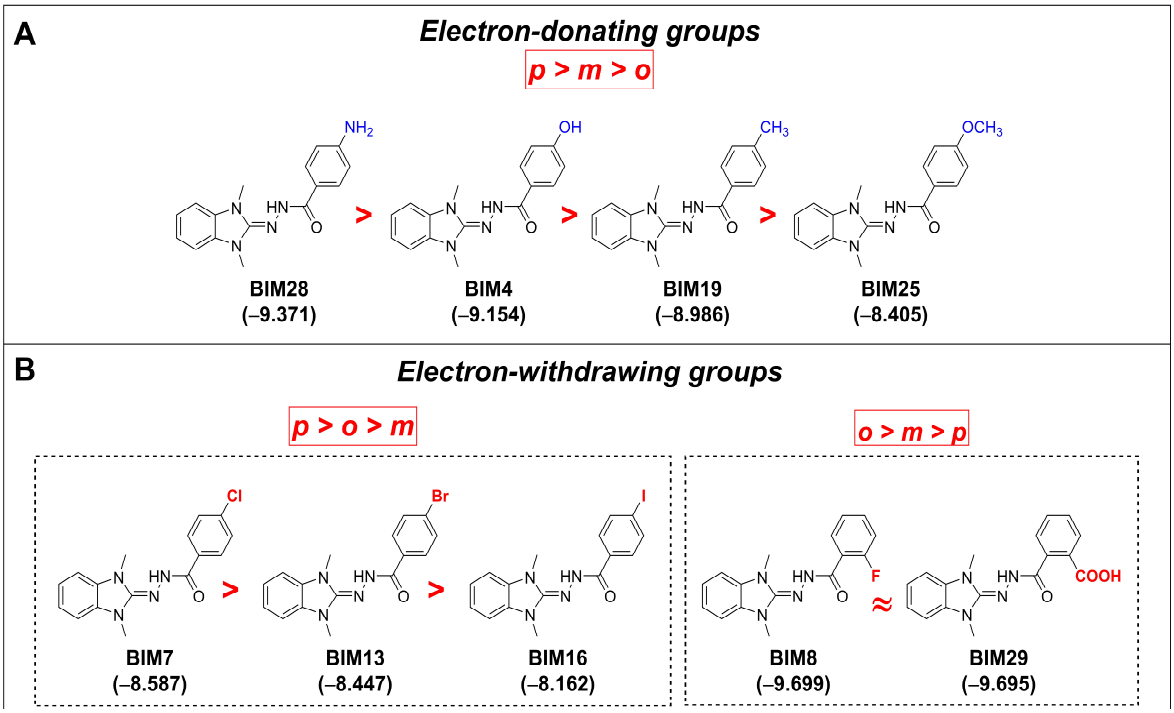

Figure 9. Docking affinity trends among substituted phenyl BIM analogues bearing **(A)** electron-donating and **(B)** electron-withdrawing groups.

Overall, the SAR analysis indicated that para substitution was generally beneficial for most electron-donating and electron-withdrawing substituents. However, strongly electronegative or highly polar substituents such as fluoro and carboxyl groups at the ortho position exhibited the highest docking affinities in the series, highlighting the importance of substituent-specific electronic and positional effects in governing ligand accommodation within the LasR binding pocket.

4.2. Molecular Properties

The top-ranked benzimidazole derivatives identified through molecular docking were further evaluated for their physicochemical and pharmacokinetic properties in order to assess their drug-like potential (**Table 3**). Physicochemical parameters including molecular weight, hydrogen bond donor and acceptor profile (donorHB and acceptHB), lipophilicity (QPlogPo/w), water solubility (QPlogS), and polar surface area (PSA) were determined. In addition, ADME-related parameters such as Caco-2 cell permeability (QPPCaco), blood–brain barrier partition coefficient (QPlogBB), and predicted human oral absorption were evaluated to estimate the absorption, membrane permeability, and oral bioavailability potential of the designed benzimidazole derivatives. Compliance with Lipinski's Rule of Five was also assessed.

remaining well within the desirable range for orally active small molecules. The QPlogPo/w values ranged from 3.30 to 4.63, indicating moderate to high lipophilicity. Compounds bearing less polar aromatic substituents, such as **BIM19, BIM10, BIM8**, and **BIM9**, showed comparatively higher lipophilicity, which may support their accommodation within the hydrophobic LasR binding pocket. The predicted aqueous solubility values (QPlogS) for all top-ranked compounds were found within the acceptable range (−6.5 to 0.5), varying from −4.59 to −5.70, indicating acceptable aqueous solubility characteristics for the designed benzimidazole derivatives. The balanced lipophilicity and aqueous solubility observed for the BIM series may be attributed to the presence of a hydrophobic benzimidazole scaffold in combination with the polar hydrazide linker.

All top ranked compounds complied with Lipinski's rule of five without any violations, indicating suitable drug-like characteristics. These compounds exhibited molecular weights ranging from 280.32 to 324.33 Da, Hydrogen-bond donor and acceptor profiles were optimal, which is important for both receptor interaction and oral bioavailability. Topological polar surface area (PSA) values ranged from 50.94 to 94.27 $Å^2$, remaining significantly below the critical threshold of 140 $Å^2$, thereby indicating favourable passive membrane permeability and efficient oral absorption. In the designed benzimidazole derivatives, the hydrazide linker and nitrogen-containing heterocyclic moieties primarily contribute to these characteristics.

The ADME-related parameters also demonstrated promising pharmacokinetic characteristics. Predicted intestinal permeability values (QPPCaco) were notably high for most compounds (ranging from 141.78 to

2691.19 nm/s), especially **BIM8, BIM9, BIM10, BIM1,** and **BIM19**, which exhibited Caco-2 permeabi-

Table 3. Physicochemical properties and predicted ADME parameters of the top 10 ranked benzimidazole derivatives.

ID	donor HB	accept HB	QPlogP$_{o/w}$	QPlogS	PSA (Å^2)	QPPCaco (nm/s)	QPlogBB	% Oral absorption	Rule of 5
Optimum range	0-6	2-20	−2.0 to 6.5	−6.5 to 0.5	7–200	>500: v. good <25: poor	–3.0 to 1.2	0–100%	0-4
BIM8	1	2	4.55	−5.41	50.94	2691.216	−0.092	100	0
BIM29	2	4	3.82	−4.70	94.27	142.231	−0.923	87.82	0
BIM9	1	2	4.55	−5.46	51.68	2475.885	−0.106	100	0
BIM52	2	3.5	3.81	−5.26	79.54	1177.541	−0.58	100	0
BIM54	1	4	3.83	−5.02	75.55	1801.925	−0.372	100	0
BIM28	2.5	3	3.30	−4.59	77.94	649.363	−0.869	96.62	0
BIM10	1	2	4.55	−5.47	51.64	2484.895	−0.104	100	0
BIM1	1	2	4.31	−5.11	51.64	2484.838	−0.213	100	0
BIM4	2	2.75	3.52	−4.71	74.20	754.451	−0.8	100	0
BIM19	1	2	4.64	−5.70	51.65	2522.328	−0.225	100	0

-lity values exceeding 2400, indicating excellent membrane permeability and absorption characteristics. Consistent with these findings, the predicted human oral absorption values were exceptionally high, with most compounds showing 100% absorption, while **BIM29** and **BIM28** also demonstrated good absorption values of 87.82% and 96.62%, respectively. Similarly, the predicted blood–brain barrier partition coefficient (QPlogBB) values ranged from −0.92 to −0.09, remaining within the acceptable range for drug-like molecules and reflecting balanced CNS permeability characteristics without excessively high brain penetration potential.

Altogether, the molecular property analysis suggested that the top docked benzimidazole derivatives possess favourable drug-like characteristics along with promising pharmacokinetic profiles. The combination of strong docking affinity, balanced lipophilicity and solubility, high predicted oral absorption, and compliance with Lipinski's criteria supports their potential as promising candidates for further development as quorum sensing inhibitors targeting the LasR receptor.

5. CONCLUSIONS

In this study, a series of benzimidazole derivatives was designed and evaluated *in silico* as potential quorum sensing inhibitors targeting the LasR receptor of *P. aeruginosa*. Molecular docking studies revealed that compounds **BIM8, BIM29, BIM9, BIM52**, and **BIM54** exhibited the highest binding affinity toward the LasR ligand-binding domain, surpassing the native autoinducer OdDHL, and established key interactions with conserved residues such as Arg61, Asp73, Tyr56, and Ser129. Analysis of structure-binding affinities revealed that both the nature of the terminal heteroaryl/aryl ring and substituent pattern significantly influenced binding affinity, with tetrazole, benzimidazole, and hydrophobic aromatic substituents showing particularly favourable interactions.

Furthermore, molecular property and ADME evaluation indicated that the top-ranked compounds possess drug-like characteristics, balanced lipophilicity, acceptable solubility, high predicted membrane permeability, and excellent oral absorption profiles, while complying with Lipinski's rule of five. Overall, the present study identifies benzimidazole as a promising scaffold for the development of LasR-targeted quorum sensing inhibitors and provides valuable structural insights for further optimization, synthesis, and biological evaluation of these derivatives as potential antivirulence agents against *P. aeruginosa*.

ACKNOWLEDGEMENTS

A. Bankar is thankful to University Grants Commission (UGC), New Delhi, India for providing Junior Research Fellowship (JRF) and Senior Research Fellowship (SRF).

REFERENCES

1. Reig S, Le Gouellec A, Bleves S. What Is New in the Anti–Pseudomonas aeruginosa Clinical Development Pipeline Since the 2017 WHO Alert? Frontiers in Cellular and Infection Microbiology. 2022;12:909731. DOI: 10.3389/fcimb.2022.909731.
2. Qin S, Xiao W, Zhou C, et al. Pseudomonas aeruginosa: Pathogenesis, virulence factors, antibiotic resistance, interaction with host, technology advances and emerging therapeutics. Signal Transduction and Targeted Therapy. 2022;7(1):199. DOI: 10.1038/s41392-022-01056-1.
3. Papenfort K, Bassler BL. Quorum sensing signal–response systems in Gram-negative bacteria. Nature Reviews Microbiology. 2016;14(9):576-588. DOI: 10.1038/nrmicro.2016.89.
4. Lee J, Zhang L. The hierarchy quorum sensing network in Pseudomonas aeruginosa. Protein and Cell. 2015;6(1):26-41. DOI: 10.1007/s13238-014-0100-x.

5. Soukarieh F, Williams P, Stocks MJ, Cámara M. Pseudomonas aeruginosa quorum sensing systems as drug discovery targets: Current position and future perspectives. Journal of Medicinal Chemistry. 2018;61(23):10385-10402. DOI: 10.1021/acs.jmedchem.8b00540.
6. Rodríguez-Urretavizcaya B, Vilaplana L, Marco MP. Strategies for quorum sensing inhibition as a tool for controlling Pseudomonas aeruginosa infections. International Journal of Antimicrobial Agents. 2024;64(5):107323. DOI: 10.1016/j.ijantimicag.2024.107323.
7. Starkey M, Lepine F, Maura D, et al. Identification of anti-virulence compounds that disrupt quorum-sensing regulated acute and persistent pathogenicity. PLoS Pathogens. 2014;10(8):e1004321. DOI: 10.1371/journal.ppat.1004321.
8. Kitao T, Lepine F, Babloudi S, et al. Molecular insights into function and competitive inhibition of Pseudomonas aeruginosa multiple virulence factor regulator. mBio. 2018;9(1):e02158-17. DOI: 10.1128/mBio.02158-17.
9. Moore JD, Gerdt JP, Eibergen NR, Blackwell HE. Active efflux influences the potency of quorum sensing inhibitors in Pseudomonas aeruginosa. ChemBioChem. 2014;15(3):435-442. DOI: 10.1002/cbic.201300701.
10. Srinivasarao S, Nandikolla A, Nizalapur S, et al. Design, synthesis and biological evaluation of 1,2,3-triazole based 2-aminobenzimidazoles as novel inhibitors of LasR dependent quorum sensing in Pseudomonas aeruginosa. RSC Advances. 2019;9(40):23389-23404. DOI: 10.1039/C9RA05059K.
11. Fuentes-Gutiérrez A, Curiel-Quesada E, Correa-Basurto J, Martínez-Muñoz A, Reyes-Arellano A. N-heterocycles scaffolds as quorum sensing inhibitors: Design, synthesis, biological and docking studies. International Journal of Molecular Sciences. 2020;21(24):9512. DOI: 10.3390/ijms21249512.
12. Abd El-Aleam RH, Sayed AM, Taha MN, George RF, Georgey HH, Abdel-Rahman HM. Design and synthesis of novel benzimidazole derivatives as potential Pseudomonas aeruginosa anti-biofilm agents inhibiting LasR: Evidence from comprehensive molecular dynamics simulation and in vitro investigation. European Journal of Medicinal Chemistry. 2022;241:114629. DOI: 10.1016/j.ejmech.2022.114629.
13. Soukarieh F, Mashabi A, Richardson W, et al. Design, synthesis, and evaluation of new 1H-benzo[d]imidazole based PqsR inhibitors as adjuvant therapy for Pseudomonas aeruginosa infections. Journal of Medicinal Chemistry. 2024;67(2):1008-1023. DOI: 10.1021/acs.jmedchem.3c00973.
14. Mohammed EZ, Rateb HS, Helwa AA, et al. Design, regioselective, time gated synthesis of novel benzo[d]imidazole analogues as potential quorum sensing inhibitors targeting LasR in Pseudomonas aeruginosa. Bioorganic Chemistry. 2026;171:109561. DOI: 10.1016/j.bioorg.2026.109561.
15. Skovstrup S, LeQuement ST, Hansen T, et al. Identification of LasR ligands through a virtual screening approach. ChemMedChem. 2013;8(1):157-163. DOI: 10.1002/cmdc.201200434.